Acta Crystallographica Section D
Biological Crystallography
ISSN 0907-4449

Structure of a new polymorphic monoclinic form of human transthyretin at 3 Å resolution reveals a mixed complex between unliganded and T_4-bound tetramers of TTR

Andrzej Wojtczak,[a] Piotr Neumann[a] and Vivian Cody[b]*

[a]Institute of Chemistry, Nicolas Copernicus University, 87-100 Torun, Poland, and [b]Hauptman–Woodward Medical Research Institute Inc., 73 High Street, Buffalo, NY 14203, USA

Correspondence e-mail: cody@hwi.buffalo.edu

Received 14 December 2000
Accepted 9 April 2001

PDB Reference: co-crystal of apo transthyretin and transthyretin–thyroxine complex, 1ict.

The crystal structure of a new polymorphic form of human transthyretin (hTTR) with a lattice containing a unique assembly of apo hTTR and TTR–T_4 complex has been determined to 3 Å resolution. The monoclinic form of human TTR reported here crystallizes in space group $P2_1$, with unit-cell parameters a = 76.7 (6), b = 96.7 (8), c = 81.7 (4) Å, β = 106.8 (4)°. The asymmetric unit contains two tetramers of transthyretin related by the non-crystallographic symmetry (NCS) operation of a 90.28° rotation between two hTTR molecules around an axis close to crystallographic z. The r.m.s. difference between the two tetramers calculated from their C^α positions is 0.48 Å. The structure was refined using 15.0–3.0 Å resolution data to R = 22.9% and R_{free} = 28.9% for reflections $F > 0.0\sigma(F)$, and R = 19.7% and R_{free} = 25.8% for reflections $F > 3.0\sigma(F)$. The intermolecular interactions involve the tips of α-helices and loops around Arg21, Glu61 and Ser100 of all monomers. The electron-density maps revealed residual thyroxine (T_4) bound in only one of the two unique tetrameric TTR molecules, with an occupancy of 53%, while the second tetramer is unliganded. One thyroxine ligand is bound in a way similar to the orientations described for the orthorhombic form of the hTTR–T_4 complex. The T_4 bound in the second site is positioned similar to 3′,5′-dinitro-*N*-acetyl-L-thyronine in its hTTR complex. Differences in the size of the central channel defined by the *D*, *A*, *G* and *H* β-strands of two monomeric subunits are observed between the apo TTR and T_4-bound tetramer. The averaged distances between Ala108 C^α and its equivalent measured across each binding site are 12.34 Å for the T_4-bound and 10.96 Å for the unliganded TTR tetramer, respectively. The observed differences might reflect the mechanics of the ligand binding in the channel and possibly explain the observed negative cooperativity effect for ligand binding.

1. Introduction

Transthyretin (hTTR, previously called prealbumin) is a plasma protein produced primarily in the liver. Transthyretin circulates in plasma and cerebrospinal fluid as a 54 000 Da tetramer with four identical subunits and is responsible for much of the transport of thyroxine (3,5,3′,5′-tetraiodo-L-thyronine, T_4) or products of its enzymatic degradation. In humans, transthyretin is one of three serum proteins that transport thyroid hormones through the general circulation and is responsible for binding about 20% of the circulating thyroxine (Braverman & Utiger, 2000; Robbins, 2000). Structural data show that the TTR tetramer has molecular D_2 symmetry, with four identical subunits forming a central channel with two T_4-binding sites (Blake *et al.*, 1978) (Fig. 1).

There are two sterically equivalent binding sites for thyroxine in the TTR tetramer which differ in their relative binding affinity. The first hormone molecule binds with $K_a = 10^8\ M^{-1}$ and the second with $K_a = 10^6\ M^{-1}$ (Cheng *et al.*, 1977). Under physiological conditions, the TTR tetramer binds only one molecule of the hormone (Robbins, 2000). A mechanism of negative cooperativity has been invoked to explain differences in the binding affinity. However, this mechanism is still poorly understood.

Transthyretin is able to self-assemble and to form amyloid fibrillar structures producing neurotoxicity and organ dysfunction (Miroy *et al.*, 1996; Benson, 1989; Colon & Kelly, 1992; Kelly & Lansbury, 1994; Sipe, 1994; McCutchen *et al.*, 1995). The wild-type TTR conversion to the amyloid causes senile systematic amyloidosis (SSA), but single-point mutations are responsible for the earlier onset of amyloidosis called familiar amyloid polyneuropathy (FAP; Kelly, 1997). More than 70 naturally occurring TTR variants are known, with most of the single-point mutations found in conservative surface substitutions that do not significantly affect the structure of the binding sites but perturb either the thermodynamics or the kinetics of the folding/denaturation pathway (Kelly, 1997; Thomas *et al.*, 1995). Some mutations are not amyloidogenic, while others destabilize the tetramer, facilitating the amyloidogenic intermediate formation. Thyroxine and other ligands are reported to stabilize the tetramer and prevent the conformational changes leading to amyloid formation (Miroy *et al.*, 1996; Klabunde *et al.*, 2000). Amyloid deposits consist of insoluble protein fibrils with a diameter of 70–100 Å that have variable length and have characteristics of a β-sheet conformation. Such structures could be responsible for many properties of the amyloid, including resistance to denaturation or cleavage. The mechanism of rearrangement and dissociation of TTR to form monomeric intermediates and subsequently to form the amyloid deposits is unclear. One model proposes changes in the secondary and tertiary structure of TTR that are pH dependent (Kelly, 1997).

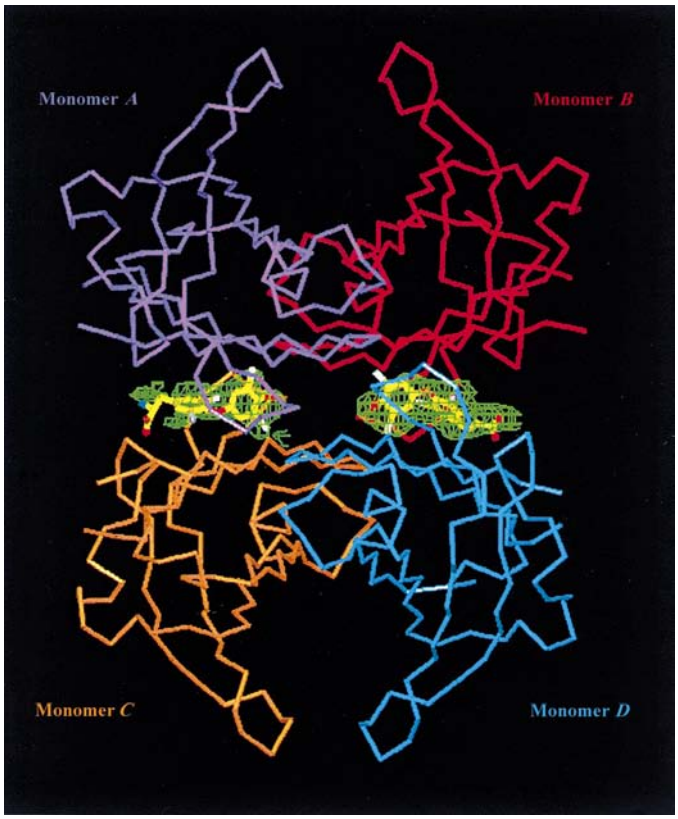

Figure 1
Monoclinic hTTR tetramer I with two T_4 ligands and the maximum-likelihood σ_A-weighted $F_o - F_c$ omit map (15.0–3.0 Å resolution, contoured at the 3σ level). The monomeric subunits of TTR, labeled *A*, *B*, *C* and *D*, form two binding sites. In the monoclinic hTTR, all four monomeric subunits are independent and two tetramers (I and II) form the asymmetric unit of the structure. In the orthorhombic form, the independent monomeric units are *A* and *B*, with two others related to *A* and *B* by crystallographic twofold symmetry (*O*, Jones *et al.*, 1997).

Structural data for human transthyretin shows that the tetramer is composed of four identical 127-residue monomers that are assembled around the central channel of the protein such that the tetramer possesses molecular D_2 symmetry (Blake *et al.*, 1978). Each monomer is a β-barrel formed by eight strands, *A* to *H*, divided into two antiparallel β-sheets, one forming the channel surface (strands *A*, *D*, *G*, *H*) and the second one on the external surface of the tetramer (strands *B*, *C*, *E*, *F*) (Blake *et al.*, 1978). Crystal structures of human TTR complexes with T_4 and its analogs, as well as native rat TTR, have been determined by X-ray crystallographic methods (Cody *et al.*, 1991; Wojtczak *et al.*, 1992, 1993, 1996; Ciszak *et al.*, 1992; De La Paz *et al.*, 1992; Hamilton *et al.*, 1993; Steinrauf *et al.*, 1993; Schormann *et al.*, 1998; Ghosh *et al.*, 2000; Sebastiao *et al.*, 1996, 1998, 2000). All structures of hTTR crystallize in the orthorhombic space group $P2_12_12$, with two independent monomers (*A* and *B*) in the asymmetric unit of the crystal lattice. The only exception is the monoclinic structure of the Leu55→Pro (L55P) variant of hTTR (Sebastiao *et al.*, 1996, 1998). In hTTR, the twofold axis coincides with the axis of the protein channel (Blake *et al.*, 1978; Blake & Oatley, 1977; De La Paz *et al.*, 1992; Cody *et al.*, 1991; Wojtczak *et al.*, 1992, 1993, 1996; Ciszak *et al.*, 1992; Hamilton *et al.*, 1993; Steinrauf *et al.*, 1993). The lack of twofold symmetry of T_4 or its competitors results in the disorder of the ligand when bound in the hTTR complex; therefore, the precise determination of the protein–ligand interactions is difficult. Rat TTR has 85% sequence homology to the human protein and has 22 amino-acid substitutions. None of the sequence differences correspond to the amino acids forming the T_4-binding site. In contrast to hTTR, the rat protein crystallizes in the tetragonal space group $P4_32_12$, with the complete tetramer in the asymmetric unit (Wojtczak, 1997). Therefore, no ligand disorder should be observed in rat TTR ligand–complex structures.

We report the X-ray crystal structure determination of a new polymorphic monoclinic form of human TTR that has two TTR tetramers in the asymmetric unit of the lattice. Analysis of these data further reveals the first example of wild-type TTR–T_4 complex with no twofold symmetry superimposed in the binding domain, as one of the tetramers has residual hormone present. Comparison of the molecular packing and

the surface regions involved in the intermolecular interactions with those found in the orthorhombic and tetragonal lattices are also described.

2. Experimental

Human transthyretin was purified as previously described (Wojtczak *et al.*, 1992) and was crystallized using the HANGMAN (Luft *et al.*, 1992; Luft & DeTitta, 1992) hanging-drop crystallization method from 55% ammonium sulfate, 0.1 *M* phosphate buffer pH 4.9. The 4 µl droplet contained 2 µl protein solution and 2 µl reservoir solution. Small crystals appeared after several weeks; however, only one crystal had a monoclinic lattice. The 3 Å resolution data were collected at 293 (1) K on a Rigaku R-AXIS II imaging-plate system for the $0.1 \times 0.1 \times 0.5$ mm monoclinic crystal and data reduction was performed using the *R-AXIS II* software. The data were analyzed for possible space-group symmetry in Laue group $2/m$. The $P2_1$ space group was assigned based on the systematic absences, with the $I/\sigma(I)$ ratio for all data and for $0k0$ reflections being 10.3 and 1.4, respectively. However, the unexpectedly low $I/\sigma(I)$ ratio of 3.2 was observed for hkl reflections with $h + k$ odd, suggested possible $C2$ symmetry. The Patterson function revealed (u, 1/2, w) peaks, as well as a (1/2, 1/2, 0) peak which was the highest peak. The volume of the unit cell corresponded to four hTTR tetramers. The parity test calculated using *DATAMAN* (Kleywegt & Jones, 1996) confirmed the pseudo-*C*-face centering, with an average $I(h + k$ odd) to $I(h + k$ even) ratio of 0.109 for all reflections. The correct assignment of the space group was also confirmed by the molecular-replacement solution, which resulted in two TTR tetramer positions in the $P2_1$ space group, while in $C2$ the tetramer of transthyretin interpenetrated its symmetry-related equivalents.

3. Molecular replacement

The molecular-replacement method as implemented in *X-PLOR* 3.1 (Brünger, 1992) was used to solve the structure with the model human hTTR tetramer generated based on the structure of the hTTR–T_4 complex (Wojtczak *et al.*, 1996; PDB code 2rox).

The Matthews coefficient of 2.64 Å^3 Da^{-1} was calculated based on the molecular weight of the transthyretin tetramer (M_r = 54 kDa), a lattice volume of 579 902 Å^3 and $Z = 4$. This value is within the limits 1.7–3.5 Å^3 Da^{-1} determined by Matthews for other protein crystal structures (Matthews, 1968) and indicates a solvent content of 53.74%. Therefore, four unique TTR tetramers can occupy this monoclinic lattice.

A self-rotation function analysis was carried out with 15.0–3.0 Å resolution data to determine the location of the non-crystallographic axes. The map section at $\varphi = 90.5^\circ$ showed two peaks and indicated two solutions of the rotation function. Examination of the section at $\varphi = 180^\circ$ (view along the y axis) showed the presence of a non-crystallographic twofold axis perpendicular to the crystallographic 2_1 axis. This confirmed that each tetramer of the monoclinic form of hTTR had non-crystallographic D_2 molecular symmetry, as expected from orthorhombic hTTR structures (Wojtczak *et al.*, 1996).

The cross-rotation function search for 15.0–3.0 Å resolution data was followed by Patterson correlation refinement (*X-PLOR*; Brünger, 1992) and showed two peaks related by rotation of 180° (φ_1) with an RF value of 0.725 and PC = 0.30 for both, which corresponded to the first TTR tetramer. The third highest peak (RF = 0.56, PC = 0.24) found in this search corresponded to the second tetramer in the asymmetric unit of the structure. These two tetramers (tetramer I and tetramer II) are related by a rotation of 90.28° about an axis close to the crystallographic z axis (the NCS axis is −23.5° from the direction of the z axis). This value was comparable with that (90.5°) resulting from the self-rotation function.

The best solution was used for an xz two-dimensional translation search for 15.0–3.0 Å resolution data in both $P2_1$ and $C2$ space groups; however, only the former was the correct solution, as indicated by the non-interpenetration of symmetry-related equivalents. The translation function T = 0.58 was 10σ above the second peak in the output, with a packing function P = 0.23. The second tetramer (in space group $P2_1$) was found in the two-dimensional xz translation search (T = 0.51, 4σ above the second peak, P = 0.19). The subsequent one-dimensional y search gave $T = 0.79$, which was higher than the second peak by 10σ and had a packing function P = 0.19.

4. Refinement

Refinement of this monoclinic hTTR structure was initiated with *X-PLOR* version 3.851 (Brünger, 1992) and continued with *CNS* (Brunger *et al.*, 1998). The manual fitting of the model into the electron-density maps was performed using *O* version 6.22 (Jones *et al.*, 1991; Jones & Kjeldgaard, 1997). 7% (899) of 14 457 reflections were set aside for use as a test set to monitor the refinement process by calculating $R_{\rm free}$ (Brünger, 1992; Kleywegt & Brünger, 1996). The $R_{\rm free}$ data set was obtained using the program *DATAMAN* (Kleywegt & Jones, 1996). In this structure, which has NCS-related molecules, the non-random way of selecting TEST reflections (Kleywegt & Jones, 1995) was used.

Rigid-body refinement of the MR solution (two tetramers followed by eight monomers) in space group $P2_1$ resulted in R = 32.9% for all data in the resolution range 8.0–3.0 Å and confirmed the space-group assignment. The subsequent refinement against data divided between the working and test sets gave R = 19.5% and $R_{\rm free}$ = 32.0% for 10 014 and 899 reflections with $F > 3.0\sigma(F)$, respectively. NCS restraints of 419 and 209 kJ mol^{-1} Å^{-1} were applied for all main-chain and side-chain atoms, respectively, and reflected the equivalence between the two tetramers in the asymmetric unit. The model was verified by calculating a series of electron-density maps averaged for two tetramers using *RAVE* (Jones, 1992; Kleywegt & Jones, 1994). Averaged electron-density maps were used during fitting both flexible and rigid regions of the protein with *O* (Kleywegt & Jones, 1999). The model was verified by calculating a series of simulated-annealing omit

Table 1
Data collection and refinement for the monoclinic human TTR.

Crystallographic data	
Space group	$P2_1$
Unit-cell parameters	
a (Å)	76.69
b (Å)	96.66
c (Å)	81.74
β (°)	106.84
Resolution (Å)	58.5–3.0
No. of independent reflections	14537
No. of observed reflections	23667
Completeness (%)	61.4
R_{merge} (%)	9.82
Highest resolution shell (Å)	3.2–3.0
$I/\sigma(I)$	4.7
Completeness	59.0
R_{merge} (%)	23.1
Refinement data	
Resolution (Å)	15.0–3.0
No. of reflections (>0.0σ)	13506/899
R/R_{free} (%)	22.9/28.9
No. of protein atoms	7176
No. of ligand atoms	48
NCS tetramers I to II coordinates (main/side) (kJ mol^{-1} Å^{-1})	42/21
NCS tetramers I to II B factors (main/side) (Å^2)	2.5/2.0
B factor (Wilson statistics) (Å^2)	10.45
Mean group B factor (r.m.s. ΔB) (Å^2)	22.28 (17.75)
Main-chain atoms (3712), tetramer I/II,	16.90/21.87
Side-chain atoms (3464), tetramer I/II	23.37/27.41
Ligand atoms (48)	49.04
R.m.s. deviations from ideality	
Bonds (Å)	0.007
Angles (°)	1.4
Dihedrals (°)	26.4
Impropers (°)	1.14
Ramachandran plot statistics	
Residues in most favored regions (%)	84.2
Residues in additional regions (%)	15.0
Residues in generously allowed regions (%)	0.8
Position error from Luzzati plot (Å)	0.30

maps. The NCS energy restraints were decreased to 209 and 84 kJ mol^{-1} Å^{-1} in order to account for conformational differences occurring in both refined tetramers of hTTR in the monoclinic $P2_1$ space group. The differences occurred initially in the most flexible regions of protein that were built differently in each tetramer (N- and C-termini, loop 33–40, loop 62–66, loop 98–103). These residues were excluded from NCS restraints during subsequent refinement. The residual was reduced to R = 16.6% and R_{free} = 26.6% for 8–3 Å 2.5σ cutoff data. The $F_o - F_c$ electron-density maps calculated on the protein model only, revealed the density corresponding to thyroxine bound in both binding sites of tetramer I. No such density corresponding to the ligand was observed in tetramer II.

The *CNS* program was used to calculate cross-validated σ_A-weighted maximum-likelihood $F_o - F_c$ maps that confirmed the position of T_4 (Fig. 1). Further refinement was carried out with the *CNS* program (Brunger *et al.*, 1998) against the maximum-likelihood target by alternate SA torsion-dynamics cycles for protein or rigid-body refinement of the ligand and manual fitting to the electron-density maps with *O*. A bulk-solvent correction was also applied and the final *CNS*-refined values were 0.235 e Å^{-3} and B = 10 Å^2. To increase the number of reflections, the 0.0σ cutoff was applied and 14 405 data in the resolution range 15.0–3.0 Å were used. These data were divided into the working set (13 506 reflections, 59.2% of all data possible to 3.0 Å resolution) and test set (899 data) selected in the non-random way (Kleywegt & Jones, 1995) as described above. Before each refinement cycle, the NCS matrix was also improved for the protein regions described above and NCS restraints of 42 and 21 kJ mol^{-1} Å^{-1} were used for the main-chain and side-chain atoms, respectively. The use of torsion dynamics reduced the number of parameters refined to 3304 (for 7224 atoms in the model). The resulting number of reflections and parameters in the working set (13 506 and 3304, respectively) had a ratio of 4.09. In order to take into account possible variation in B factors, group B factors were calculated, one for the main-chain atoms and another for the side-chain atoms of each residues, and resulted in 1858 B-factor groups refined. All the electron-density maps were cross-validated, σ_A-weighted and calculated against the maximum-likelihood target. No water molecules were included in the model. The final model consists of residues 10–125 for each monomer. Attempts to locate the missing residues 1–9 and 126–127 failed because of poorly defined electron density.

Based on the cross-validated σ_A-weighted SA omit maps (15.0–3.0 Å resolution 0.0σ cutoff data), the position of T_4 in the binding sites of tetramer I (Fig. 2) was confirmed and included in further refinement. The final refinement gave R = 22.9%, R_{free} = 28.9% for 0.0σ cutoff (15.0–3.0 Å, 13 506 working reflections and 899 test reflections), while the statistics calculated for 3.0σ cutoff data (10 397 working and 753 test reflections) are R = 19.7% and R_{free} = 25.8%. The conformational statistics show that 84.2% of residues are positioned in the most favored regions of the Ramachandran plot, 15.0% in additionally allowed regions and only seven residues (0.8%) in generously allowed regions, as calculated with the program *PROCHECK* (Laskowski *et al.*, 1993). The summary of structure solution and refinement are given in Table 1.

5. Results and discussion

This new polymorph of hTTR contains two tetramers in the asymmetric unit of the cell. Tetramer I (hTTR–T_4 complex) consists of monomers *A*, *B*, *C* and *D*. The equivalent monomeric subunits of tetramer II (apo) are denoted *A*′, *B*′, *C*′ and *D*′. The statistics on the degree of similarity of NCS-related molecules, as calculated using *LSQMAN*, *MOLEMAN*2 and the other recommended programs (Kleywegt, 1996, 1997), are presented in Table 2. A multiple-model Ramachandran plot (not shown) revealed only small differences between protein regions related by NCS.

As shown in Table 2, there are no significant differences in the polypeptide-chain conformation between the cores of two tetramers. The residues excluded from the NCS restraints differ in φ/ψ angles more than those in the core. The largest r.m.s. differences for the main-chain atom positions are

observed for the N- and C-termini and flexible-loop regions 35–40, 60–66, 98–103 of all monomers. Statistics values for NCS models (r.m.s.d. C^{α}, r.m.s.d. all atoms and $\delta\varphi/\varphi > 10^{\circ}$) calculated for the monoclinic hTTR structure are in the expected range for the class of similar structures included in the Quality Data Base (QDB). The QDB contains statistics for 476 protein entries from the PDB all of which have either been solved at low resolution or contain NCS or both (Kleywegt, 1996).

The proper NCS transformation matrix between tetramers I and II corresponds to a 90.28° rotation around the axis close to the crystallographic z axis and translation by a vector T (82.17, −19.34, −8.43 Å). The similarity of tetramers I and II, as well as the individual monomers, have been verified by r.m.s. fitting and from the NCS restraints applied during the refinement. Discrepancies observed between the refined model and the density-maps fit during refinement had limited the use of NCS restraints to the β-sheet structure – the most rigid regions of both tetramers. Therefore, the core of both tetramers has a similar conformation, while larger differences are observed in the flexible loops on the protein surface. The r.m.s. distance between C^{α} atoms is 0.48 Å, the average distance is 0.37 Å for 464 C^{α} atoms and the maximum distance is 2.16 Å. The similarity plot (not shown) (Sanchez & Sali, 1997) revealed a high degree of similarity between tetramers, with the r.m.s. distance calculated for C^{α} atoms of 409 residues (88.1%) of 0.31 Å. The r.m.s. differences calculated between the equivalent monomeric subunits of two tetramers are usually less than 1.0 Å, except between the C-termini of monomers A and A', between monomers B and B' loop 30 and loop 60 (about 1.5 Å), between monomers C and C' loop 30 and 100 (about 1.5–1.8 Å), and between monomers D and D' loops 30 and 100 (1.5–2.16 Å).

Table 2
The comparison of two monoclinic hTTR tetramers.

Values in parentheses are standard deviations.

Statistics	Average
Number of residues in the structure	930
Tetramer I	466 (two T_4 ligands)
Tetramer II	464
φ/ψ angles	
Tetramer I *versus* tetramer II	
Average $\sigma(\varphi)$ (°)	6.42 (7.88), 464 residues
Average $\sigma(\psi)$ (°)	6.25 (8.16), 464 residues
$\delta\varphi/\delta\psi$ (°)	12.73/12.39
R.m.s. φ/ψ	20.24/20.48
Residues with $\delta\varphi/\delta\psi > 10^{\circ}$	199/186
Percentage	42.89/40.09
Residues included in NCS averaging (320)	
Average $\sigma(\varphi)$ (°)	4.10 (3.33)
Average $\sigma(\psi)$ (°)	4.05 (4.95)
$\delta\varphi/\delta\psi$ (°)	10.13/7.44
R.m.s. φ/ψ	10.13/12.26
Residues with $\delta\varphi/\delta\psi > 10^{\circ}$	105/96
Percentage	32.81/30.00
Residues excluded in NCS averaging (144)	
Average $\sigma(\varphi)$ (°)	11.69 (11.71)
Average $\sigma(\psi)$ (°)	11.24 (11.20)
$\delta\varphi/\delta\psi$ (°)	19.32/18.58
R.m.s. φ/ψ	30.08/28.84
Residues with $\delta\varphi/\delta\psi > 10^{\circ}$	95/91
Percentage	65.97/63.19

6. Comparison of the two thyroxine-binding sites in tetramer I

Refinement of the monoclinic form of hTTR revealed that only tetramer I has bound two molecules of T_4 in the AC and BD binding sites. The ML simulated-annealing σ_A-weighted omit map calculated with 15.0–3.0 Å data, $0.0\sigma(F)$ cutoff (Fig. 2) and the difference Fourier maps clearly showed density for the ligand ring system with the iodine substituents in both binding sites of tetramer I. The analysis of contacts reveals that the two T_4 ligands are oriented differently in each binding site. The T_4 molecule in the BD site is bound deeper and its overall orientation is similar to that described for the hTTR complex of 3′,5′-dinitro-*N*-acetyl-L-thyronine (DNNAT; Wojtczak *et al.*, 1996). The difference between these ligand positions is a result of the absence of 3,5-substituents on the tyrosyl ring of DNNAT which increases its conformational flexibility compared with thyroxine (T_4). As a result, the phenolic ring and alanyl moiety of T_4 have similar orientations, while the orientation of the tyrosyl ring differs for the two ligands (T_4 and DNNAT). The orientation of T_4 in the AC site is similar to that described for the orthorhombic complex of hTTR (Wojtczak *et al.*, 1996), but the ligand is bound deeper by about 1.5 Å in the channel toward the tetramer center than T_4 in the orthorhombic structure. The iodine substituents of the phenolic ring occupy the pair of innermost halogen pockets P3 and P3′ (Blake & Oatley, 1977; De la Paz *et al.*, 1992). The alanyl moiety forms polar contacts with the protein side chains of Lys415 and Glu454. The differences between the two binding sites have been analyzed by comparison of the side-chain angles χ^1 and χ^2 (calculated with *LSQMAN*). Large differences (above 45°) between the AC and BD binding sites were observed for the conformation of the side chains of Lys15, Glu54, Tyr105, Ile107, Tyr116, Ser117, Met413, Lys415, Glu454, Leu455, His456, Ser512, Tyr514, Thr518 and Thr519, the amino acids that constitute the ligand-binding site. Those results are consistent with the list of ligand interactions reflecting the different T_4 binding.

7. Comparison of binding-domain size in liganded and unliganded forms

To the best of our knowledge, the size of the binding channel in the AC and BD sites of TTR has never been discussed in the published literature. The comparison of binding sites was made in terms of the interatomic distances between C^{α} atoms of equivalent amino acids measured across the TTR channel in each binding site. During the structure-determination process, two tetramers were located by the MR method using the orthorhombic hTTR tetramer as a starting model. Therefore, the AC and BD binding sites have been identified and assigned consistently with the orthorhombic hTTR structure (Wojtczak *et al.*, 1996). The distance differences across the channel have been compared between the two

binding sites of each TTR tetramer (Fig. 3). The $A'C'$ site of the unliganded tetramer II is characterized by larger distances between the A and D and the G and H β-strands; distances between residues 105–108 of strand G and 119–120 of H β-strands are smaller than in the $B'D'$ site. These differences have a 'wave pattern'. The analogous analysis performed for the T_4-bound tetramer I revealed the same trend, although the amplitude of the changes is decreased. The comparison was also made between the equivalent binding sites of tetramers I and II (Fig. 4). Analysis revealed that the ligand bound in the first site causes a decrease of the channel diameter which results from slight alterations of the channel surface. Owing to the relative rigidity of the β-sheet structure forming the channel, the second binding site appears to open enough to accommodate the second ligand molecule. The differences in the channel diameter in the second site are decreased relative to the unliganded tetramer. Therefore, the sequence of events includes the ligand binding in the first site (AC) with a slight collapse of this site and a corresponding opening of the second site, followed by binding of the second molecule and collapse of that site. The reverse process with the relative opening of the first site upon the second ligand binding is negligible owing to the bridging interactions already formed by the first ligand which increase the relative rigidity of the structure. This could explain the negative cooperativity effect of weaker binding of the second molecule to the unliganded binding site of TTR tetramer.

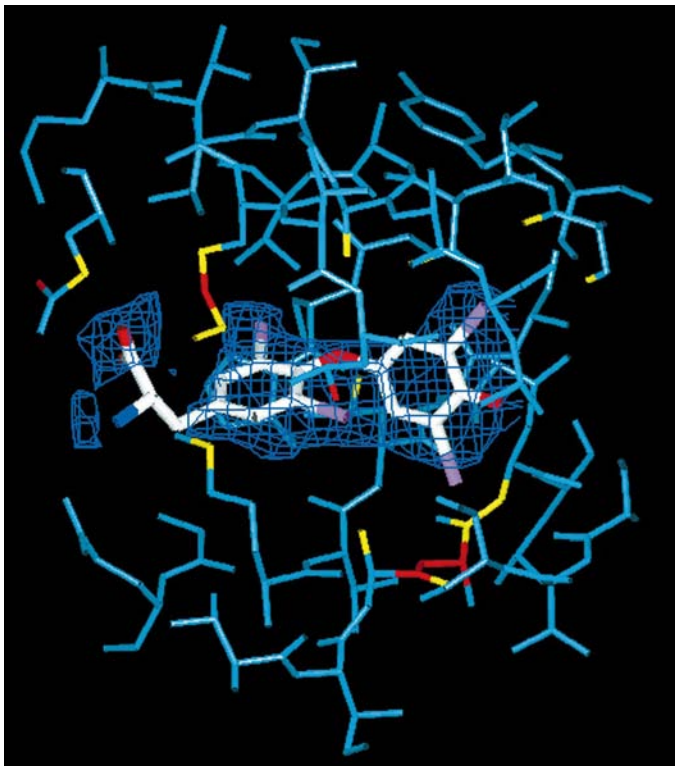

Figure 2
The maximum-likelihood σ_A-weighted simulated-annealing omit map 15.0–3.0 Å 0.0σ cutoff (contoured at 2.5σ) calculated for the AC binding site of tetramer I shows the orientation of T_4 in the channel. Protein atoms closer than 3.2 Å to the ligand are colored red, between 3.2–3.6 Å are colored yellow and those more distant are colored cyan (*O*, Jones *et al.*, 1997).

8. Comparison of monoclinic and orthorhombic hTTR with tetragonal rTTR

The conformation of the polypeptide chain for all forms of TTR (two monoclinic, orthorhombic and rat tetragonal) are similar. The r.m.s. distance of the C^{α} positions calculated between tetramers I and II of monoclinic $P2_1$ (monoP) hTTR, the orthorhombic (orth) hTTR and tetragonal rTTR (Wojtczak, 1997) are listed in Table 3. Despite similarities between all these structures, differences are observed for some of the flexible loops and the N- and C-termini. The superposition of the two tetramers of monoP hTTR, the orth hTTR and the rat TTR revealed that the largest r.m.s. distances between C^{α} atoms are in the flexible surface regions near residues 61, 100 and 38, as well as the N- and C- termini. These loop regions are known for their flexibility in all TTR struc-

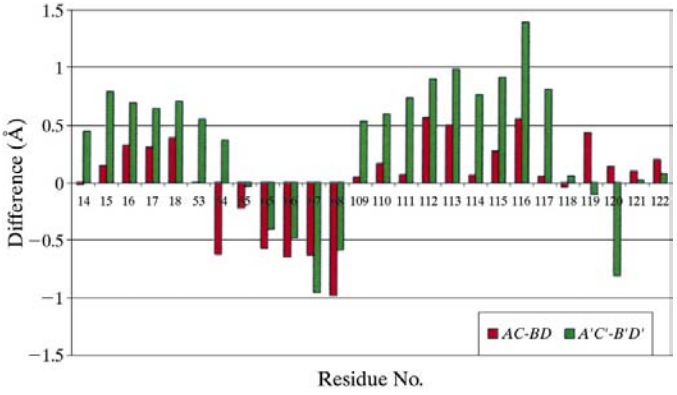

Figure 3
Comparison of the two binding sites in tetramer I (red, hTTR–T_4 complex) and tetramer II (green, apo hTTR). The differences $\delta(AC) - \delta(BD)$ and $\delta(A'C') - \delta(B'D')$ are plotted for the distances measured across the TTR channel between the equivalent residues constituting the ligand-binding site. The differences between the sites do not exceed 1.1 Å. The amplitude of changes in complex tetramer (I) is smaller than that observed for the apo tetramer (II).

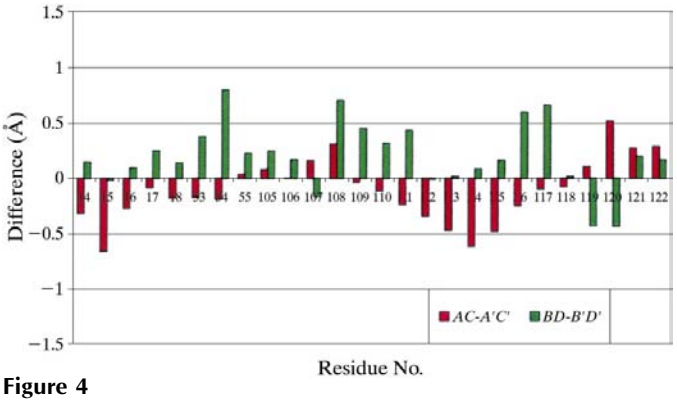

Figure 4
Comparison of two binding sites in the tetramers I (complex) and II (apo hTTR). The differences $\delta(AC) - \delta(A'B')$ (red) and $\delta(BD) - \delta(B'D')$ (green) were plotted for the distances measured across the TTR channel between the equivalent ligand-binding sites.

tures. Extensive fitting of the loops during the refinement process for monoP hTTR resulted in structures that corresponded to an averaged loop structure for the different conformers. Nevertheless, the differences in the core region observed between both human TTR polymorphs (0.62 and 0.68 Å between 2rox and tetramers I and II, respectively) are smaller than those observed between monoP hTTR and rTTR (0.70 and 0.72 Å between 1gke and tetramers I and II, respectively). Therefore, one might expect the higher r.m.s. distance to reflect the differences in the conformational space caused by the sequence differences between the human and rat proteins occurring in the protein core region and in the adjacent 60–65 regions. Also, no conformational differences are found in the T_4-binding site between two polymorphs of hTTR.

9. Comparison of crystal packing among forms of TTR

9.1. Monoclinic lattice: $P2_1$ *versus* $C2$

Two monoclinic polymorphs of hTTR have been identified: the primitive lattice observed in this structure with two independent tetramers in the asymmetric unit (Figs. 5 and 6) and a C-centered lattice observed for the L55P variant of hTTR which has two independent dimers that constitute the *CD–EF* tetramer and two independent dimers (*AB* and *GH*) that form the asymmetric unit (Sebastiao *et al.*, 1996, 1998). The twofold symmetry in the *C*2 space group generates the tetramers from the two independent dimers. Consequently, the structure is made up of three different types of tetramers, two of which have only their halves as symmetry-independent units. There is no symmetry operation in this space group to form a unique tetramer from the two independent dimers of the L55P hTTR structure.

Analysis of the packing of these two polymorphs shows that they each have different arrangements of the tetramers in their respective lattices. Although the packing arrangement of the tetramers differ, the monoP structure shows evidence of pseudo-*C*-centering (Figs. 7 and 8). Both independent tetramers of the monoP hTTR structure form sublattices of layers parallel to the (001) plane, with pseudo-centering corresponding to an $a + b/2$ translation relating the pairs of non-equivalent monomers. In the sublattice formed by tetramer I the pseudo-centering relates monomers *A* to *C* and *B* to *D* of the adjacent tetramers, while in the sublattice formed by tetramer II, translation relates monomers A' to B' and C' to D'. Since there are differences in the conformation of the flexible loops between the eight monomers within the asymmetric unit, the pseudo-centering causes a significant reduction in the intensities of the *hkl* reflections for $h + k$ odd [mean $I/\sigma(I)$ ratio 3.2] but does not result in real systematic absences. As described earlier, the lattice type for this structure was validated as primitive.

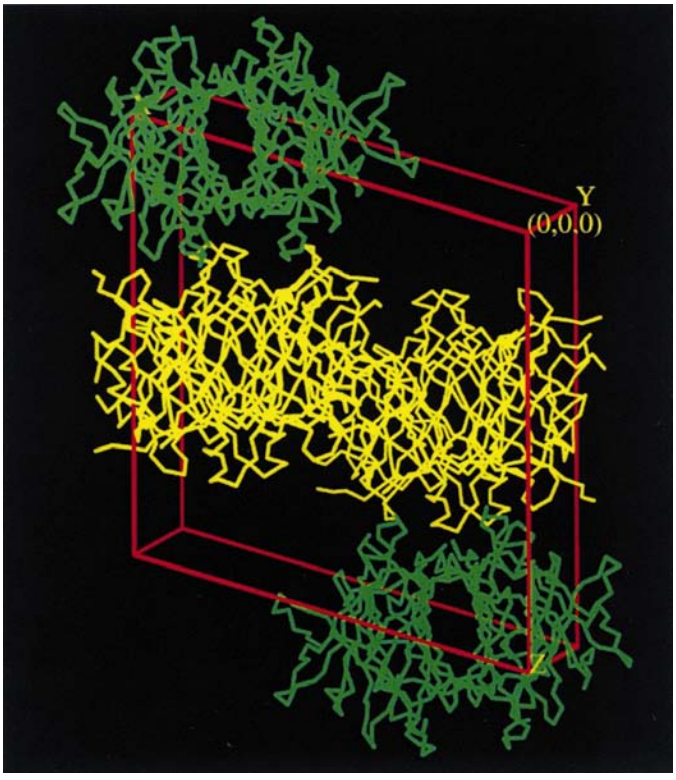

Figure 5
The packing diagram for monoclinic hTTR projected along the *y* axis. Tetramers I are colored yellow and tetramers II are shown in green. The channel axis of the tetramer II is parallel to the crystallographic *y* direction. The axis of the tetramer I channel is approximately perpendicular to this direction.

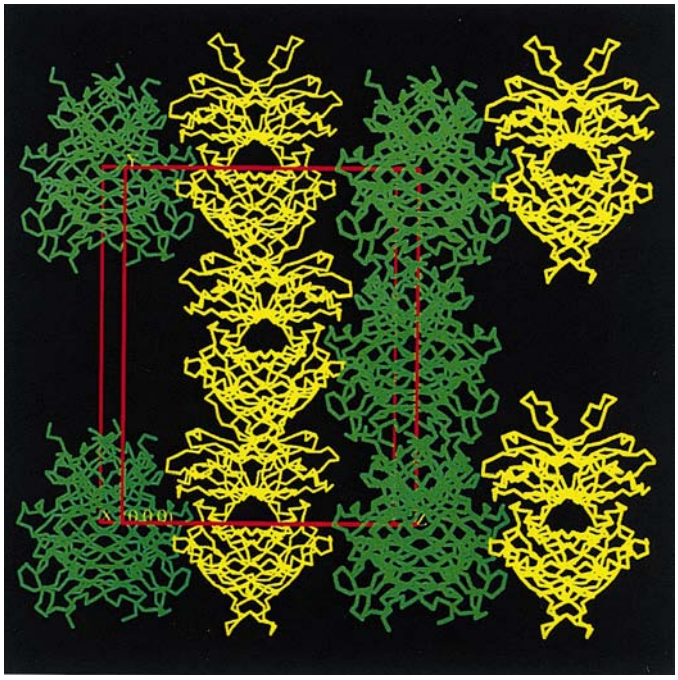

Figure 6
The packing diagram projected along the crystallographic *x* axis, which is parallel to the channel axis of the tetramer I. The structure is made up of alternate layers of tetramer I (yellow) and tetramer II (green) which are parallel to the (001) plane. The NCS operation between tetramers I and II corresponds to a rotation of 90.28° around a direction close to the *z* axis (*O*, Jones *et al.*, 1997).

Table 3
The intermolecular interactions found in three forms of TTR.

+ indicates regions involved in the intermolecular interactions. ++ indicates regions interacting with their structural equivalents. * indicates the position of amyloid-related mutations changing the properties of the amino acids.

	hTTR $P2_12_12$		rTTR $P4_32_12$		hTTR $P2_1$			
Z, V_M (Å^3 Da^{-1})	2, 2.23		8, 2.58		4, 2.64			
pH	5.5		5.0		4.9			
R.m.s.d. (Å) between TA and TB	C^α 0.848, C^α 0.891		C^α 0.885, C^α 0.898		C^α 0.480			
Layer orientation	(100)		(001)		(001)		(001)	
Tilt out of the layer plane	~4° from (100)		~5° from (001)		Tetramer I ~24° from (001)		Tetramer II ~23° from (001)	
Residues	Monomers I–I	Monomers II–II	Intralayer	Interlayer	Tetramer I Intralayer	Interlayer I–II	Tetramer II Interlayer II–I	Intralayer
20–27	—	—	—	+	—	+	+	—
31–33*	+	+	+	—	+	—	—	+
34–40*	—	—	++	—	+	—	—	+
41–46*	+	+	++	—	+	—	—	—
47–49*	+	—	+	—	—	—	—	+
51–53*	—	—	+	—	—	—	—	—
54–55*	—	—	+	—	—	—	—	+
56–59*	—	—	++	—	—	—	—	+
60–62*	+	+	+	—	+	—	—	+
63–64*	+	+	—	—	+	—	—	+
65–66	+	+	—	—	+	—	—	—
72–74	+	+	—	—	—	—	—	—
77–79*	—	+	—	—	—	—	—	—
80–85*	—	—	—	++	—	++	++	—
89–90*	—	—	+	—	—	—	—	—
98–103	—	+	—	++	+	++	++	+
124–126	—	—	+	+	—	—	—	+

9.2. Comparison of crystal packing between three forms of TTR

Two kinds of molecular layers that contain only one tetramer (I or II) form sublattices in the monoP crystal. The tetramers positioned in two different layers of TTR molecules are rotated by 90.28° relative to each other around an axis close to the crystallographic z direction (Fig. 5). This rotation is calculated as the NCS symmetry operator used during the refinement. The network of interlayer interactions between tetramers I and II involve the same surface regions of the four monomeric subunits: Arg34, the loop region 62–66, residues 81–85 at the C-terminus of the only α-helix, residues 98–103 and a few residues from the N- and C-termini of both tetramers (Table 3). The C-terminal fragments of the α-helices from adjacent molecules that penetrate the shallow cleft between the helices on the side surface of the other tetramer, forming a cluster of four 81–84 and 98–103 loops. Such an arrangement is similar to that observed in the tetragonal lattice of rTTR (Wojtczak, 1997), but is not observed in the orthorhombic form of hTTR.

The $C2$ crystal lattice of L55P hTTR is made with two types of alternating layers. The first layer is formed by two dimers (*CD–EF*) constituting the tetramer with a relative tilt out of the layer plane of about 32.4°. The second layer is made up of two tetramers that are formed from the two independent dimers (*AB* and *GH*). These two tetramers differ slightly in orientation and reveal a different tilt out of the layer (26.8 and 33.2° for the $ABA'B'$ and $GHG'H'$ tetramers, respectively).

The asymmetric unit of the monoP hTTR lattice consists of two unique tetramers which reveal no twofold molecular symmetry. In contrast to the L55P TTR variant, the layers of molecules are formed by TTR tetramers of identical orientation. The alternating layers in this structure are formed by tetramers of hTTR rotated by approximately 90° relative to each other and the packing of tetramers is not as compact as observed for the L55P TTR structure. This is also reflected in the Matthews coefficient of 2.64 Å^3 Da^{-1} (Matthews, 1968), which is slightly larger than the value of 2.60 Å^3 Da^{-1} reported for L55P TTR (Sebastiao *et al.*, 1996, 1998). Despite these differences, the intermolecular interactions and crystal packing are similar in both structures. The network of interlayer interactions between the tetramers involve the same surface regions of the four monomeric subunits: loop region 62–66, residues 81–85 at the C terminus of the only α-helix, residues 98–103 and a few residues from the N- and C-termini. The C-terminal fragments of the α-helices from the adjacent molecules penetrate the shallow cleft between the helices on the side surface of the other tetramer, forming a cluster of four 81–84 and 98–103 loops. Such an arrangement is similar to that observed in the tetragonal lattice of rTTR (Wojtczak, 1997), but is not observed in the orthorhombic form of the hTTR–T_4 complex (Wojtczak *et al.*, 1996).

9.3. Orthorhombic human TTR

In the orthorhombic lattice, hTTR tetramers form layers parallel to the crystallographic (100) plane with intralayer packing interactions involving the external surfaces of the 30–45 strand–loop–strand fragments. These layers are similar to those formed by tetramers I and II in this monoP hTTR structure. The intermolecular space in each layer in orth hTTR

is filled with the molecules of the next layer ($n + 1$) translated along the [011] diagonal. Interlayer interactions are established between the nth and ($n + 2$)th layer tetramers and involve the C-terminal fragments of the α-helices (interacting tip-to-tip) on both side surfaces of TTR tetramer. Such an arrangement of TTR molecules in the lattice is described by orthorhombic $P2_12_12$ symmetry.

9.4. Tetragonal rat TTR

In rat TTR, the crystal lattice is formed from the tetramer layers perpendicular to the crystallographic z [001] axis (Wojtczak, 1997), with interactions involving both internal and external surfaces of the 30–45 strand–loop–strand fragments. The fragments from the A and B monomers form a four-loop connection with the C and D monomers of the symmetry-related tetramer; the tip of the domain B loop is positioned between similar fragments in domains C and D of another TTR. The intralayer interactions are found mainly between loops 31–45 of monomers B and D, while for the analogous regions of monomers A and C only a few contacts were found. The layers are also assembled *via* the interactions involving four-subunit interfaces on the side surfaces of the tetramers; however, these interactions differ from those found in this human TTR structure. These non-equivalent interactions result in a different number of contacts shorter than 3.5 Å. The adjacent layer is rotated 90° with respect to the crystallographic z axis and results in a series of contacts along the surface of the tetramer. In rTTR the C-termini of the α-helices penetrate the cavities between corresponding fragments and β-turn fragments 111–114 on the adjacent tetramer, reaching deeper towards the β-turn residues 19–22 at the bottom of the cavity. The interlayer interactions for rat TTR are similar to those described for the structure of monoclinic hTTR reported here. In Table 3, the interactions between different layers of TTR tetramers are defined in the monoclinic hTTR and the tetragonal rTTR. In the structure of orthorhombic hTTR, the same regions are involved in the intra- and inter-layer interactions owing to the packing observed in the $P2_12_12$ space group.

Sebastiao *et al.* (1998) suggested that the crystal packing found in L55P TTR might be similar to the TTR amyloid fiber structure. The only significant differences in the monomer and tetramer geometry between the L55P variant and the wild-type hTTR structures are found around Pro55 and of these residues only the fragment 60–63 is involved in intermolecular interactions. Channels similar to those described in the L55P TTR packing are also found in wild-type hTTR reported here, as well as the orthorhombic human and tetragonal rat TTR structures (Wojtczak, 1997). The L55P TTR structure crystallized at pH 7.5, while the monoclinic wild-type hTTR crystallized at pH 4.9. Nevertheless, the structure reported here reveals surprisingly similar packing to that of the L55P variant. Therefore, we conclude that a pH change of 2.6 units

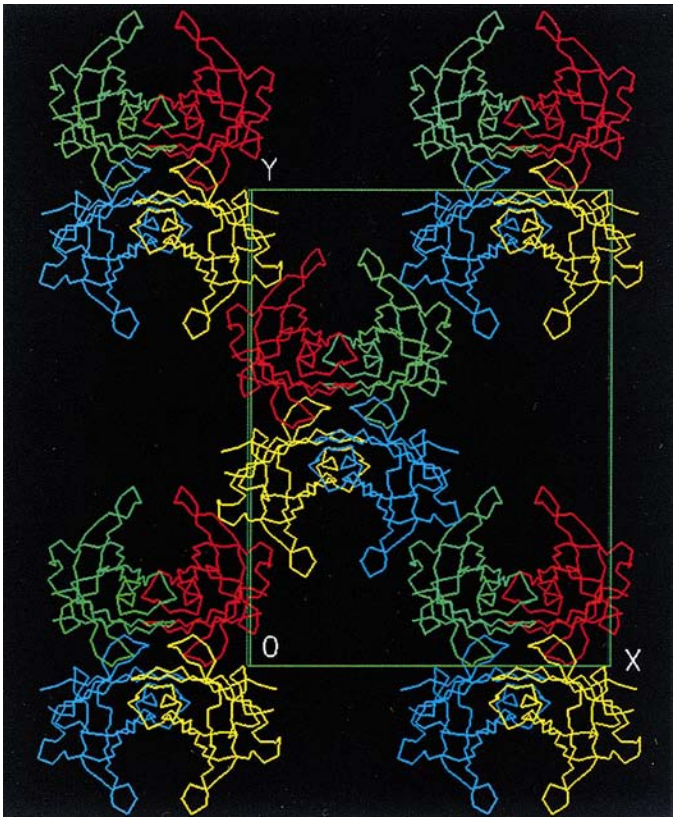

Figure 7
The packing environment of tetramer I of the monoclinic lattice (*SETOR*; Evans, 1993) projected down the z axis shows pseudo-C-centering. The monomers A, B, C and D are colored red, green, yellow and cyan, respectively.

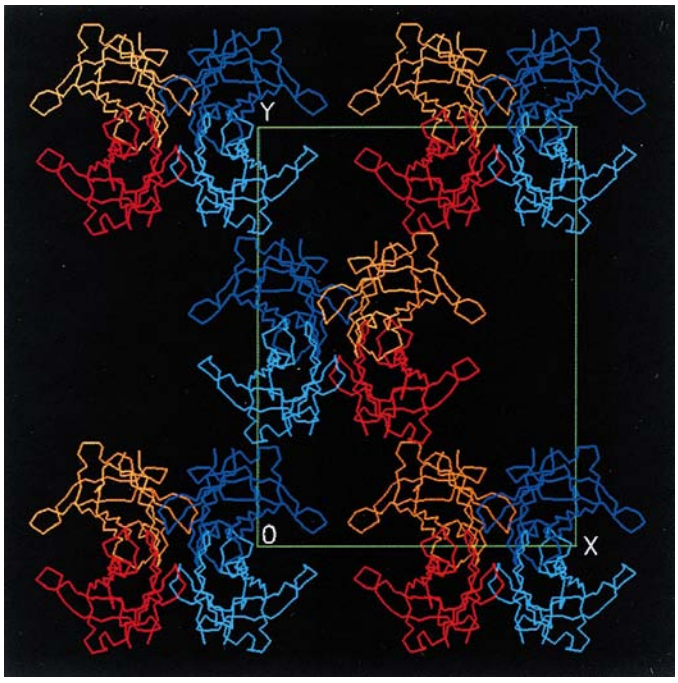

Figure 8
The packing environment of tetramer II of the monoclinic lattice (*SETOR*; Evans, 1993) projected along the z axis also shows pseudo-C-centering. The monomers A', B', C' and D' are colored cyan, blue, red and orange, respectively.

cannot significantly alter the TTR packing resulting from the interactions formed by the surface polar groups. This conclusion was also made from a comparison of published TTR structures and a higher resolution wild-type hTTR (Hornberg *et al.*, 2000). However, rat TTR crystallized at pH 5.0 shows a different packing (Wojtczak, 1997) owing to the surface characteristics altered by the multiple sequence differences. Consequently, the ability of transthyretin to undergo the transition into the amyloid fiber seems to be an intrinsic property of this protein and is only assisted by the destabilizing effects of a particular mutation.

10. Conclusions

This structure determination reveals no significant differences in the polypeptide-chain conformation between the monoclinic hTTR and the orthorhombic hTTR or tetragonal rTTR structures. Crystal packing in this monoclinic polymorph of hTTR is intermediate between that observed for the orthorhombic hTTR and tetragonal rTTR structures. Monoclinic hTTR tetramer I forms interlayer interactions that are similar to those of orthorhombic hTTR, while tetramer II participates in interlayer interactions that are analogous to rTTR (clusters of helical tips). Monoclinic hTTR reveals no clustering of loops 30–40 which was characteristic of rTTR. The monoclinic hTTR tetramers reveal a different tilt from the layer plane to that described for other forms of TTR. In all three forms of transthyretin (monoP hTTR, orth hTTR, rTTR) the intermolecular interactions involve the 30–45, 56–63 and 98–103 regions, in which a number of FAP-related mutations are known to occur. The thermodynamic preferences for these surface regions suggest their potential importance for intermolecular interactions and possibly their role in association during the FAP amyloid formation, which is enhanced by the decrease in the monomer and tetramer stability. The amyloid formation is known to be pH induced, although no significant differences in the polypeptide chain conformation were associated with differences in the pH of crystallization. Therefore, the differences observed in crystal-packing interactions related to the crystallization conditions (pH, ionic strength) might provide insight into the preferred regions of the tetramer surface that could be engaged in the fibril association.

This research was supported in part by grants from Polish KBN 6/P04A/032/11 (AW) and NIH-Fogarty FIRCA TW00789 (VC). The authors thank Joe Luft and Dan Cotter for crystallization, and Walt Pangborn for data collection.

References

Benson, M. D. (1989). *Trends Biochem. Sci.* **12**, 88–92.
Blake, C. C. F., Geisow, M. J., Oatley, S. J., Rerat, B. & Rerat, C. (1978). *J. Mol. Biol.* **11**, 339–356.
Blake, C. C. F. & Oatley, S. J. (1977). *Nature (London)*, **268**, 115–120.
Braverman, L. E. & Utiger, R. D. (2000). Editors. *The Thyroid, A Fundamental and Clinical Text*, 8th ed. Philadelphia: J. B. Lippincott.
Brünger, A. (1992). *X-PLOR Version* 3.1. *A System for X-ray Crystallography and NMR*. New Haven: Yale University Press.
Brunger, A. T., Adams, P. D., Clore, G. M., DeLano, W. L., Gros, P., Grosse-Kunstleve, R. W., Jiang, J.-S., Kuszewski, J., Nilges, M., Pannu, N. S., Read, R. J., Rice, L. M., Simonson, T. & Warren, G. L. (1998). *Acta Cryst.* D**54**, 905–921.
Cheng, S. Y., Pages, R. A., Saroff, H. A., Edelhoch, H. & Robbins, J. (1977). *Biochemistry*, **16**, 3707–3713.
Ciszak, E., Luft, J. & Cody, V. (1992). *Proc. Natl Acad. Sci. USA*, **89**, 6644–6648.
Cody, V., Wojtczak, A., Ciszak, E. & Luft, J. (1991). *Progress in Thyroid Research*, edited by A. Gordon, J. Gross & G. Hennemann, pp. 793–796. Rotterdam: Balema.
Colon, W. & Kelly, J. W. (1992). *Biochemistry*, **31**, 8654–8660.
De La Paz, P., Burridge, J. M., Oatley, S. J. & Blake, C. C. F. (1992). *The Design of Drugs to Macromolecular Targets*, edited by C. R. Beddell, pp. 119–172. New York: Wiley & Sons, Inc.
Evans, S. V. (1993). *J. Mol. Graph.* **11**, 134–138.
Ghosh, M., Meerts, I. A. T. M., Cook, A., Bergman, A., Brouwer, A. & Johnson, L. N. (2000). *Acta Cryst.* D**56**, 1085–1095.
Hamilton, J. A., Steinrauf, L. K., Braden, B. C., Liepniks, J., Benson, M. D., Holmgren, G., Sandgren, O. & Steen, L. (1993). *J. Biol. Chem.* **268**, 2416–2424.
Hornberg, A., Eneqvist, T., Olofsson, A., Lundgren, E. & Sauer-Eriksson, A. E. (2000). *J. Mol. Biol.* **302**, 649–669.
Jones, T. A. (1992). *Proceedings of the CCP4 Study Weekend. Molecular Replacement*, edited by E. J. Dodson, S. Gover & W. Wolf, pp. 91–105. Warrington: Daresbury Laboratory.
Jones, T. A. & Kjeldgaard, M. (1997). *Methods Enzymol.* **277**, 173–208.
Jones, T. A., Zou, J. Y., Cowan, S. W. & Kjeldgaard, M. (1991). *Acta Cryst.* A**47**, 110–119.
Kelly, J. W. (1997). *Structure*, **5**, 595–600.
Kelly, J. W. & Lansbury, P. T. J. (1994). *Amyloid*, **1**, 186–205.
Klabunde, T., Petrassi, H. M., Oza, V. B., Raman, P., Kelly, J. W. & Sacchetti, J. C. (2000). *Nature Struct. Biol.* **7**, 312–321.
Kleywegt, G. J. (1996). *Acta Cryst.* D**52**, 842–857.
Kleywegt, G. J. (1997). *J. Mol. Biol.* **273**, 371–376.
Kleywegt, G. J. & Brünger, A. T. (1996). *Structure*, **4**, 897–904.
Kleywegt, G. J. & Jones, T. A. (1994). *Proceedings of the CCP4 Study Weekend. From First Map to Final Model*, edited by S. Bailey, R. Hubbard & D. Waller, pp. 59–66. Warrington: Daresbury Laboratory.
Kleywegt, G. J. & Jones, T. A. (1995). *Structure*, **3**, 535–540.
Kleywegt, G. J. & Jones, T. A. (1996). *Acta Cryst.* D**52**, 826–828.
Kleywegt, G. J. & Jones, T. A. (1999). *Acta Cryst.* D**55**, 941–944.
Laskowski, R. A., MacArthur, M., Moss, D. S. & Thornton, J. M. (1993). *J. Appl. Cryst.* **26**, 283–291.
Luft, J. R., Cody, V. & DeTitta, G. T. (1992). *J. Cryst. Growth*, **122**, 181–185.
Luft, J. R. & DeTitta, G. T. (1992). *J. Appl. Cryst.* **25**, 324–325.
McCutchen, S. L., Lai, Z., Miroy, G. J., Kelly, J. W. & Colon, W. (1995). *Biochemistry*, **34**, 13527–13536.
Matthews, B. W. (1968) *J. Mol. Biol.* **33**, 491–497.
Miroy, G. J., Lai, Z., Lashuel, A., Peterson, S. A., Strang, C. & Kelly, J. W. (1996). *Proc. Natl Acad. Sci. USA*, **93**, 15051–15056.
Robbins, J. (2000). *The Thyroid, A Fundamental and Clinical Text*, 8th ed., edited by L. E. Braverman & R. D. Utiger, pp. 105–120. Philadelphia: J. B. Lippincott.

Sanchez, R. & Sali, A. (1997). *Proteins Struct. Funct. Genet. Suppl.* **1**, 50–58.
Schormann, N., Murrell, J. R. & Benson, M. D. (1998). *Amyloid Int. J. Exp. Clin. Invest.* **5**, 175–187.
Sebastiao, M. P., Dauter, Z., Saraiva, M. J. & Damas, A. M. (1996). *Acta Cryst.* D**52**, 566–568.
Sebastiao, M. P., Merlin, G., Saraiva, M. J. & Damas, A. M. (2000). *Biochem. J.* **351**, 273–279.
Sebastiao, M. P., Saraiva, M. J. & Damas, A. M. (1998). *J. Biol. Chem.* **273**, 24715–24722.
Sipe, J. D. (1994). *Crit. Rev. Clin. Lab. Sci.* **31**, 325–354.
Steinrauf, L. K., Hamilton, J. A., Braden, B. C., Murrell, J. R., Benson, M. D., Holmgren, G., Sandgren, O. & Steen, L. (1993). *J. Biol. Chem.* **268**, 2425–2430.
Thomas, P. J., Qu, B.-H. & Pederson, P. L. (1995). *Trends Biochem. Sci.* **20**, 456–459.
Wojtczak, A. (1997). *Acta Biochim. Pol.* **44**, 505–518.
Wojtczak, A., Cody, V., Luft, J. R. & Pangborn, W. (1996). *Acta Cryst.* D**52**, 758–765.
Wojtczak, A., Luft, J. R. & Cody, V. (1992). *J. Biol. Chem.* **267**, 353–357.
Wojtczak, A., Luft, J. R. & Cody, V. (1993). *J. Biol. Chem.* **268**, 6202–6206.